ARTICLE IN PRESS

Available online at www.sciencedirect.com

SCIENCE DIRECT

ELSEVIER

Journal of Computational Physics xxx (2005) xxx–xxx

JOURNAL OF COMPUTATIONAL PHYSICS

www.elsevier.com/locate/jcp

The force/work differencing of exceptional points in the discrete, compatible formulation of Lagrangian hydrodynamics

R. Loubère *, E.J. Caramana

T-7 and CCS-2, Los Alamos National Laboratory, Theoretical Division, T7, MS B284, Los Alamos, NM 87545, United States

Received 21 December 2004; received in revised form 8 June 2005; accepted 15 November 2005

Abstract

This study presents the force and mass discretization of exceptional points in the compatible formulation of Lagrangian hydrodynamics. It concludes a series of papers that develop various aspects of the theoretical exposition and the operational implementation of this numerical algorithm. Exceptional points are grid points at the termination of lines internal to the computational domain, and where boundary conditions are therefore not applied. These points occur naturally in most applications in order to ameliorate spatial grid anisotropy, and the consequent timestep reduction, that will otherwise arise for grids with highly tapered regions or a center of convergence. They have their velocity enslaved to that of neighboring points in order to prevent large excursions of the numerical solution about them. How this problem is treated is given herein for the aforementioned numerical algorithm such that its salient conservation properties are retained. In doing so the subtle aspects of this algorithm that are due to the interleaving of spatial contours that occur with the use of a spatially-staggered-grid mesh are illuminated. These contours are utilized to define both forces and the work done by them, and are the central construct of this type of finite-volume differencing. Additionally, difficulties that occur due to uncertainties in the specification of the artificial viscosity are explored, and point to the need for further research in this area.

Keywords: Lagrangian; Hydrodynamics; Energy conserving; High speed flow; Artificial viscosity

1. Introduction

Most physical applications that involve Lagrangian or ALE hydrodynamics calculations employ grids that must be unstructured to some degree to avoid the spatial grid stiffness that would otherwise occur, resulting in an unacceptable decrease in timestep. While the problem of differencing the hydro equations about exceptional, or irregular, points of such grids has been addressed in a previous paper for the case where the exact one-dimensional symmetry limit is desired in curvilinear coordinates [1], the solution presented requires rotations of the force that may not be desirable for general cases, particularly those where low-dimensional symmetry is not important and does not attain to any approximate degree in the solution. However, the general

* Corresponding author. Tel.: +1 505 667 1407.
E-mail addresses: loubere@lanl.gov (R. Loubère), ejc@lanl.gov (E.J. Caramana).

0021-9991/$ - see front matter
doi:10.1016/j.jcp.2005.11.022

discussion given therein of the timestep vicissitudes of such grids remains valid and is not repeated here. An example of the type of grid previously considered is shown in Fig. 1. Here the terminated lines, and associated exceptional points, are displayed as hollow circles that are placed at the midpoints of straight lines connecting neighboring regular points. This is opposed to being placed on a common radius as previously depicted in [1]. It is in general necessary to enslave the terminated points shown in Fig. 1 to prevent large unphysical perturbations in the solution from occurring about them when disturbances such as shock waves propagate in any direction across them. Thus the force and mass discretizations that are suitable for regular zones that do not contain these points must be appropriately modified where they are present in the grid. This requires a careful investigation of the discretization properties of the underlying hydro algorithm that elucidates all assumptions, transparent or hidden. To this end, Section 2 gives a brief review of the hydro algorithm that forms the title of this paper. This is, however, a new and concise presentation that displays essential features that complement previous expositions [2,3].

In Section 3 the types of grids encountered are briefly detailed as well as the basic constraints that are enforced when both mass and force from the exceptional points are "donated" to neighbors to which their velocity is enslaved, making the former "nondynamical". Section 4 gives numerical results that validate the discretization rules introduced in Section 3, and quantifies the magnitude of errors that necessarily occur when strong shock waves encounter these points. In particular, special attention is paid to the artificial viscosity forces as they are velocity dependent; and since velocity interpolation is utilized, these forces can result in sensitivities that are difficult to counter by any general prescriptions. Last, a discussion of this work and its principal conclusions is given.

2. Discrete, compatible Lagrangian hydrodynamics

The discrete, compatible formulation of Lagrangian hydrodynamics [3] essentially modernizes older forms of Lagrangian hydro [4]. It places this type of numerical algorithm into a simple and consistent framework where conservation of total energy plays the central role, but where the principal dependent variables remain density, velocity, and specific internal energy. Like all the older versions of Lagrangian hydrodynamics it employs a staggered grid in space with velocity and position carried on points "p", and density, specific internal energy, and stress centered in zones "z". However, both zones and points are considered to be surrounded by interleaved volumes circumscribed by lines in 2D (or surfaces in 3D) that are termed the "coordinate-line" and "median" meshes, respectively, as shown in Fig. 2. This interleaved topology allows for a simple finite-volume calculation of forces. These act from zones that carry a mass M_z, and onto points that carry a mass M_p, where "z" and "p" are integer indices that range over all zones and points, respectively. Auxiliary quantities denoted as "corner" masses and forces are introduced; these are unique and common to both a zone and a given point of that zone, and thus carry both the zone and the point indices. The zone and point masses and the total force acting on a point are then constructed from these more primitive entities as simple sums. The corner mass is denoted as m_z^p or m_p^z, and the corner force as $\vec{f}_z^{\,p}$ or $\vec{f}_p^{\,z}$, where the lower index denotes that which

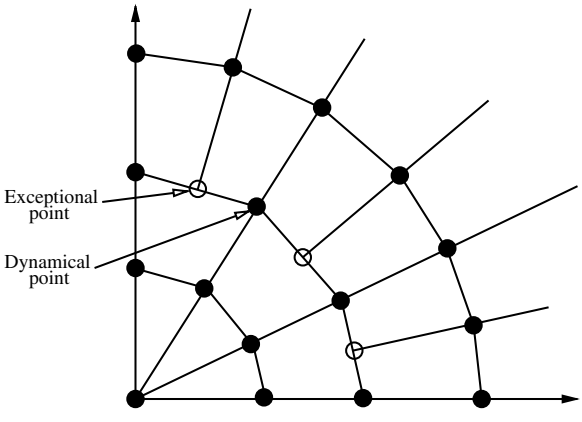

Fig. 1. Typical mesh with exceptional points. Exceptional points are enslaved to adjacent dynamical points on an angular grid line.

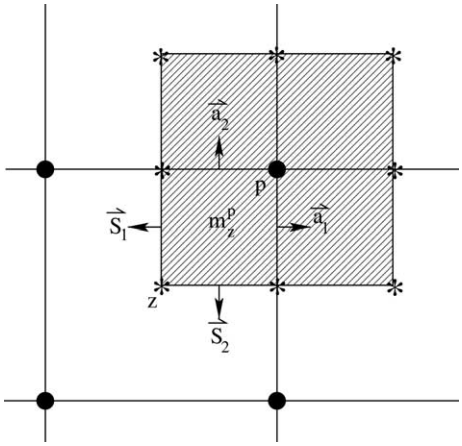

Fig. 2. Coordinate-line mesh thru solid dots; median mesh thru stared points: subcell geometrical vectors $\vec{a}_1, \vec{a}_2, \vec{S}_1, \vec{S}_2$ associated with zone "z"; m_z^p is corner mass.

is summed, but they are otherwise equal. The corner forces mediate the exchange of kinetic and internal energy from points to zones, or vice-versa.

The essentials of this algorithm can be presented in a very succinct form that displays both its power and simplicity in the following manner: consider the change in the kinetic energy of a point "p" between two time levels "n" and "$n+1$" as given by $\Delta K_p \equiv M_p[(\vec{v}_p^{n+1})^2 - (\vec{v}_p^n)^2]/2$ in a timestep Δt. Then note that the difference in the squares of the point velocity, $\vec{v}_p$, between the two time levels can be uniquely factored to yield

$$\Delta K_p = M_p \Delta \vec{v}_p \cdot \Delta \vec{r}_p / \Delta t, \tag{2.1}$$

where $\Delta \vec{v}_p \equiv (\vec{v}_p^{n+1} - \vec{v}_p^n)$, and more importantly the change in the position vector, $\vec{r}_p^n$, is $\Delta \vec{r}_p \equiv (\vec{v}_p^{n+1} + \vec{v}_p^n)\Delta t/2$. That is, the reason the coordinates are advanced as $\vec{r}_p^{n+1} = \vec{r}_p^n + \Delta \vec{r}_p$ with the just specified form for $\Delta \vec{r}_p$ is not to obtain second order accuracy in time (other forms may give higher order), but because of the manner in which the kinetic energy difference between two time levels factors! Defining the change in internal energy in a zone in a time Δt as $M_z \Delta e_z$, where $\Delta e_z \equiv (e_z^{n+1} - e_z^n)$, and summing the change of kinetic energy over all points "p", and the change in internal energy over all zones "z", the change in total energy on a timestep, ΔE, can be written as

$$\Delta E \equiv \sum_p M_p \Delta \vec{v}_p \cdot \Delta \vec{r}_p / \Delta t + \sum_z M_z \Delta e_z = \Delta W_{\mathrm{bd}}, \tag{2.2}$$

where ΔW_{bd} is the boundary work performed on the particular timestep. Next the momentum and specific internal energy equations are "postulated" to have the discrete forms

$$M_p \Delta \vec{v}_p = \sum_z \vec{f}_z^p \Delta t, \tag{2.3}$$

where the sum of the arbitrary corner force is over all zones that contain point "p", and

$$M_z \Delta e_z = -\sum_p \vec{f}_p^z \cdot \Delta \vec{r}_p, \tag{2.4}$$

where this sum is over all points that circumscribe zone "z". Note that what has been done is to define the total force that acts on a point "p" as the sum of all corner forces that act from zones adjacent to that point; and also, to define the work done into a zone "z" as the negative sum of the corner forces of that zone dotted into their respective point displacements on the given timestep. For example, for the case of pressure forces this sum is a discrete form of $-P_z \Delta V_z$ work, where P_z is the zone pressure and ΔV_z is the change in zone volume in a timestep.

Writing the momentum equation in the form given by Eq. (2.3) may appear to be simply a useful division of the force acting on a point into single contributions from surrounding zones. However, that the work

performed by a zone can be written as Eq. (2.4) utilizing the same corner forces such that this work becomes a simple sum of corner force times point displacement is more significant, as this guarantees exact conservation of total energy for forces of completely arbitrary origin. Note that the force of gravity exchanges kinetic energy with gravitational potential energy and thus does not enter into the corner force; but rather, enters directly as an additional term on the RHS of the momentum equation, and with the kinetic energy of a point augmented by its gravitational potential in the total energy tally. Likewise, Eq. (2.4) can contain an additional source term on the RHS that originates from the direct deposition of internal energy from chemical or other sources.

To demonstrate energy conservation suppose that the momentum equation, Eq. (2.3), is dotted into the point displacement on a timestep, $\Delta\vec{r}_p$, and its RHS inserted into the first sum in Eq. (2.2). Then the RHS of Eq. (2.4) is likewise inserted into the second sum of Eq. (2.2). This results in

$$\Delta W_{\mathrm{bd}} = \sum_p \sum_z \vec{f}_z^{\,p} \cdot \Delta\vec{r}_p - \sum_z \sum_p \vec{f}_p^{\,z} \cdot \Delta\vec{r}_p, = \sum_{p=\mathrm{bd}} \sum_{z=\mathrm{ext}} \vec{f}_z^{\,p} \cdot \Delta\vec{r}_p. \tag{2.5}$$

Since the corner force is unique to a given zone and point of that zone (recall that $\vec{f}_z^{\,p} = \vec{f}_p^{\,z}$), the second sum from the internal energy equation completely cancels with terms from the first sum due to the momentum equation. There remains only terms that sum over the boundary points "$p = \mathrm{bd}$" from the external zones "$z = \mathrm{ext}$" that lie adjacent to these points that form the prescribed boundary; these terms define the boundary work performed on the given timestep. Thus total energy is conserved exactly in that when integrated in time Eq. (2.2) yields $E^n = E^{n=0} + W^n_{\mathrm{bd}}$, where $E^{n=0}$ is the initial total energy and W^n_{bd} is the sum of the boundary work as given by Eq. (2.5) over all timesteps to the final time "t^n". Total energy is also conserved locally in that the internal domain of interest can consist of any collection of zones, or just a single zone. This latter case is illustrated in Fig. 3 where a single 2D quadrilateral zone "z" is shown with its associated corner forces "$\vec{f}_i^{\,z}$", and where "$i = 1 \ldots 4$" ranges over its defining points. For this case $E^n = M_z e^n_z + \sum_{i=1}^4 M_i (\vec{v}_i^{\,n})^2/2$. Defining "$\vec{F}_i$" as the sum of all corner forces that act on point "$p = i$" in a timestep, it follows from Eq. (2.5) that the boundary work performed on a timestep is $\Delta W_{\mathrm{bd}} = \sum_{i=1}^4 (\vec{F}_i - \vec{f}_i^{\,z}) \cdot \Delta\vec{r}_i$. This is the total exterior work performed with respect to any single zone. If there is no mass exterior to the boundary, the sum of all zone masses and the sum of all point masses are equal (a consistency requirement), but otherwise this is not true and is not necessary for total energy to be conserved.

As previously noted [3], the discrete form of the equations for total energy, momentum, and internal energy when written as Eqs. (2.2)–(2.4) constitute an algebraic identity; given any two, the third uniquely follows. This identity employs three totally arbitrary entities referred to as the zone mass, M_z, the point mass, M_p, and the corner force ($\vec{f}_z^{\,p}$ or $\vec{f}_p^{\,z}$). It is the proper specification of these otherwise abstract objects that gives this system physical meaning; however, whatever their specification the quantity defined above as "total energy" is always exactly conserved. The program of the rest of the development of the discrete, compatible formulation

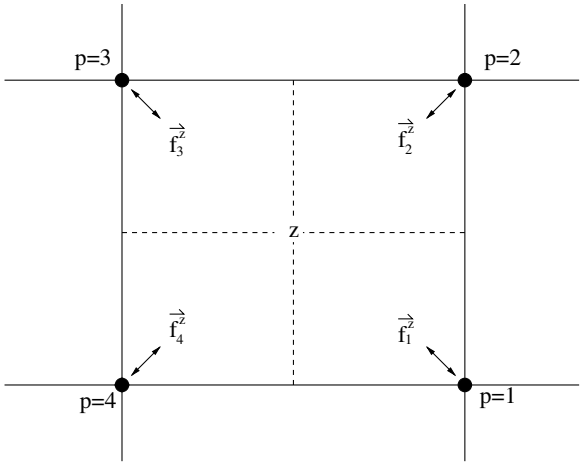

Fig. 3. Single quadrilateral zone "z" with its defining points p_1, p_2, p_3, p_4, and associated corner forces $\vec{f}_p^{\,z}$, $1 \leqslant i \leqslant 4$.

of Lagrangian hydrodynamics is to specify these three objects. The word "discrete" is to be emphasized in that these equations are considered to describe the time evolution of small fluid volumes, as opposed to a differencing of the equations of continuum fluid dynamics.

The nodal and zonal masses, M_p and M_z, are straightforwardly constructed by introducing the corner mass m_z^p or m_p^z, where the zone mass is simply the sum of all m_p^z's over points about the specified zone "z"; and likewise, the point mass M_p is the sum of all m_z^p's over all zones adjacent to point "p" [3]. The median mesh is hinged by auxiliary points, shown as asterisks in Fig. 2, that are determined by time independent interpolation coefficients (usually $1/2, 1/4, \ldots$) applied to neighboring dynamical points. That these coefficients be time independent is necessary to prevent destructive nonlinear feedback between the median and coordinate-line meshes. The specification of the corner force is much more involved, and is given for regular zones in both 2D and 3D for all force contributions: mean zone stress, artificial viscosity, and anti-hourglass forces in a series of previously published papers [3,5–9]. Although this corner force specification is given as a form of finite volume differencing, other discretizations can be utilized to define the corner forces. It is the purpose of this work to extend the finite volume definitions to the aforementioned case of exceptional points that preserve not only conservation of total energy, but also the conservation properties of Eqs. (2.2)–(2.4) that the original corner force specifications enforce. The nature of these are briefly detailed.

Principal amongst the additional conservation laws is the conservation of linear momentum, which can be stated most succinctly as the homogeneity of space (referred to as Noether's theorems [10]). This adheres for our discrete equations as follows: suppose that a constant but arbitrary displacement vector, "$\vec{r}_0$", is added to the coordinates of all points in space by performing a Galilean boost, $\vec{v}_0$, such that $\vec{r}_0 = \vec{v}_0 \Delta t$ during any given timestep. Then for the discrete form of the internal energy equation, Eq. (2.4), to remain unchanged it is required that

$$\sum_z \vec{f}_z^{\,p} \cdot \vec{r}_0 = \vec{r}_0 \cdot \sum_z \vec{f}_z^{\,p} = 0. \tag{2.6}$$

Thus the requirement of linear momentum conservation is just the statement that all corner forces in a zone must sum to zero. For zones with a constant stress throughout the entire zone, this means that the zone volume is closed and simply connected so that the sum of its surface area vectors equal zero. (Note that for 1D cylindrical or spherical geometry this requirement does not hold since these zone volumes, as formed by two concentric circles or spheres, are not simply connected.) Conservation of angular momentum, as the isotropy of space, follows similarly as requiring $\sum_p \vec{r}_p \times \vec{f}_p^{\,z} = 0$ in each zone, where $\vec{r}_p$ is the position vector to a point "p" from any arbitrary origin of the coordinate system. All corner forces are required to obey conservation of linear momentum on a single zone basis when cast into Cartesian geometry. This property is central to our treatment of exceptional points; however, not all force contributions obey angular momentum conservation on a single zone basis if they arise from stresses that are not constant throughout a given zone. This is true for both the subzone-pressure anti-hourglass forces [6], and the edge-centered artificial viscosity forces [5]. However, studies have shown that global breaking of angular momentum conservation remains at small truncation error levels for these force contributions. Finally, for the stated system of equations to give useful results they must be time advanced in a numerically stable manner. This is achieved by a predictor-corrector step where the predictor and corrector stages are identical except that the corner forces are centered at the "n" time level on the predictor, and at the "$n + 1/2$" time level on the corrector, resulting in second order accuracy in time and numerical stability subject to the usual CFL constraint [1].

3. Finite-volume mass/force/work computation

The basic program of this work is to give a general prescription of how to perform the force and mass discretizations about exceptional points of terminated lines as shown in Fig. 1. However, this may not be for the simple terminations shown; instead these may consist of a line of such points in two or in three dimensions. It is not our purpose to detail all possible cases, but instead, to give some general rules that enable one to adapt the basic underlying differencing to any situation, and to illustrate the general method and show its effectiveness for certain relevant cases. The central idea is to treat all points as though they are regular, then the exceptional points have their associated corner forces and masses appropriately "donated" to points to which their

velocity is enslaved. One must examine the character of the individual contributions to the corner force to ascertain that they still behave in a physically meaningful manner. First, the kind of zone topologies encountered with the exceptional points of terminated lines must be considered.

Two types of median mesh configurations that can occur in 2D geometry for the exceptional point "p_e" are shown in Fig. 4. If this point is considered to be a defining point of all zones, as is the case in Fig. 4(a), then the large zone on the left is a degenerate pentagon; whereas in Fig. 4(b), this point belongs to the smaller rectangles on the right but is not considered a defining point for the large zone on the left, which remains a quadrilateral. Since the lines that comprise the median mesh connect midpoints of the coordinate lines to the zone center point, the subzone corner volumes appear skewed to one side if the exceptional (termed "nondynamical" from hereon) point is considered part of the larger zone. Thus the light gray region in Fig. 4(a) denotes the three corner masses that are associated with point "p_e" if it were to remain dynamical. Our first alteration from the usual definitions used to construct the median mesh is to erase the nondynamical point from being associated with the large zone on the left in Fig. 4. All corner forces are thus constructed from the mesh shown in Fig. 4(b). The nondynamical point "p_e" now obtains mass only from the two small corner volumes of the rectangular zones of Fig. 4(b) shown as the light gray region, and no mass from the larger zone to its left that no longer identifies it as a part of that zone; the same statement holds for the corner forces. Next, three basic principles are enunciated that determine how to difference about any one or any set of nondynamical points:

1. Corner masses are donated from nondynamical points such that, aside from convergence effects, corner volumes are matched in size about dynamical points that neighbor nondynamical ones.
2. Corner forces are donated from nondynamical points to neighboring dynamical points such that force equilibrium is achieved for uniform stress in a region about these points.

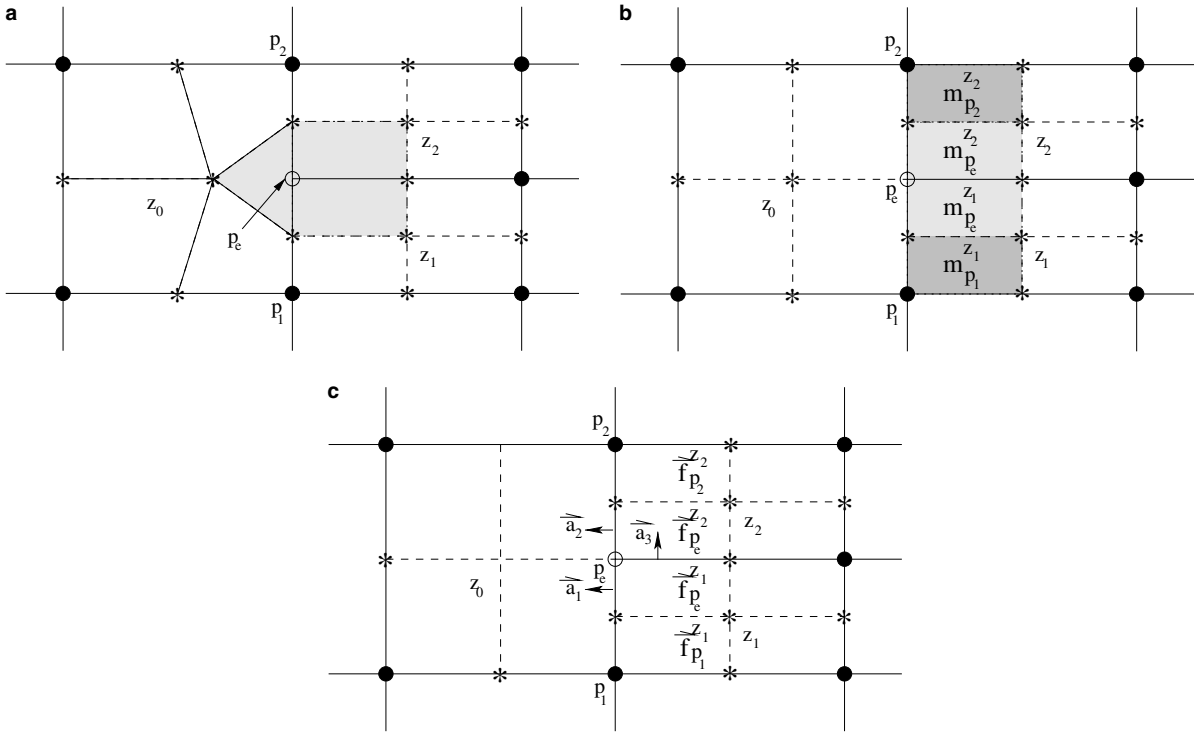

Fig. 4. (a) Exceptional point p_e, shown as "○", is considered as a dynamical point for the large zone z_0 and the smaller zones z_1, z_2; Subcells of point p_e are light gray regions. The median mesh is plotted with dashed lines, the coordinate-line mesh with solid lines. (b) Exceptional point p_e considered a dynamical point for only for the smaller zones z_1, z_2. The subcell associated with p_e in zone z_0 no longer exists. The dark gray subcells are the ones to which the remaining masses/forces of point p_e are donated, m_p^z is the mass of subcell associated with zone z and point p. (c) Coordinate-line mesh area vectors $\vec{a}_i$, $1 \leqslant i \leqslant 3$, associated with the subcell force donations and subcell forces $\vec{f}_p^z$.

3. Conservation of linear momentum as defined by Eq. (2.6) must be maintained for all zones. This generalizes the definition of the term "zone".

The consequences of these three requirements are now examined.

The basic idea behind the first of our three statements is readily seen from Fig. 4(b). To make the corner volume and corner mass on the right side of the two dynamical points "p_1" and "p_2" match that from the large zone on the left of these points, one must let $m_{p_1}^{z_1} \rightarrow m_{p_1}^{z_1} + m_{p_e}^{z_1}$ and $m_{p_2}^{z_2} \rightarrow m_{p_2}^{z_2} + m_{p_e}^{z_2}$. Next one sets both $m_{p_e}^{z_1}$ and $m_{p_e}^{z_2}$ equal to zero, so that the nondynamical point "p_e" carries no mass; thus it does not contribute kinetic energy to the total energy tally.

The requirement of equilibrium for uniform stress demands that the two corner forces that act on point "p_e" from zones "z_1" and "z_2" first be summed, then one-half of this sum is donated to points "p_1" and "p_2". That these corner forces must be summed before being donated can be seen from the fact that for a uniform pressure "P" in zones "z_1", "z_2" and "z_0", $\vec{f}_{p_e}^{z_1} = P(\vec{a}_1 + \vec{a}_3)$ and $\vec{f}_{p_e}^{z_2} = P(\vec{a}_2 - \vec{a}_3)$. (Here the grid vectors $\vec{a}_i$ are oriented as shown in Fig. 4(c) and have magnitudes of the length of the half-edges to which they are normal.) By adding these two corner forces the term associated with the grid vector $\vec{a}_3$ cancels. Thus when this sum is donated to the dynamical points "p_1" and "p_2" with simple factors of one-half to each, force equilibrium is achieved when taking into account the corner force contribution from the large zone, "z_0", that lies to the left side of these points. That is, we define $\vec{F}_{p_e} \equiv \vec{f}_{p_e}^{z_1} + \vec{f}_{p_e}^{z_2}$ and then let $\vec{f}_{p_1}^{z_1} \rightarrow \vec{f}_{p_1}^{z_1} + \vec{F}_{p_e}/2$, $\vec{f}_{p_2}^{z_2} \rightarrow \vec{f}_{p_2}^{z_2} + \vec{F}_{p_e}/2$. Last, we set $\vec{f}_{p_e}^{z_1}$ and $\vec{f}_{p_e}^{z_2}$ to zero and can proceed with zone sweeps as before to assemble the total force on all points.

The sum of the original corner forces add to zero individually in the two rectangular zones of Fig. 4(b) that contain the nondynamical point "p_e". However, because of the sum and then division performed to satisfy the requirement of force equilibrium for uniform pressure, zones "z_1" and "z_2" must now be considered as a single composite zone when the internal energy equation, Eq. (2.4), is solved. That is, the sum of the corner forces of both of these zones still sum to zero, but no longer on a single zone basis. Thus the change of specific internal energy, Δe_z, due to the corner forces acting in these two zones must be considered as a single sum. This is because by donating the force from the nondynamical point, the grid vectors that make up the force contours sum to zero only over the composite region "$z_1 + z_2$". If there are no other energy sources in Eq. (2.4), and if both regions "z_1 and "z_2" have equal specific internal energies at time zero, then this equality is maintained for later time. However, even in this case the pressure in these two zones need not be equal since their zone densities can still have different values.

The velocity enslavement of nondynamical points always utilizes a simple linear interpolation to neighboring dynamical points. This serves to keep the position of these points closely synchronized to dynamical ones preventing large spatial excursions that would otherwise occur. Thus for the case shown in Fig. 4(b), $\vec{v}_{p_e} = (\vec{v}_{p_1} + \vec{v}_{p_2})/2$, keeping the enslaved point "p_e" at the midpoint of the line connecting points "p_1" and "p_2".

The procedure just outlined can be extended to two or more terminated lines with associated nondynamical points between two dynamical points, to which their velocities are enslaved by linear interpolation, in a completely analogous manner. The large zone adjacent to the terminated lines is again made into a quadrilateral, and all its corner forces are computed the same as for any other quad. Corner volumes are donated to the two dynamical points such that corner volume matching is achieved with respect to the large zone. Corner forces are summed on the terminated line side and then donated to the dynamical points with coefficients that are the same as used to donate the nodal volume/mass. (That is, a single nondynamical point may now contribute all of its nodal mass and force to a single dynamical point, instead of one-half to each.) Likewise in 3D, although the situation may be more complicated to visualize, the manner in which the nondynamical points of terminated lines are treated is not fundamentally different than in 2D; the three principles given above are applied to all situations using a linear interpolation of the velocity from the dynamical to the nondynamical points.

The artificial viscosity forces that appear in these equations must be given special consideration as these forces are velocity dependent, and thus do not compose about nondynamical points in the same manner as the total stress and anti-hourglass forces that are completely accounted for by the above set of rules. However, in the calculations shown in the next section they are treated the same as all other forces since the basic algorithm consists of assembling the corner force from all the various contributions and then manipulating the

corner force as previously described. Two different forms of artificial viscosity are utilized: an edge-centered form [5] and a tensor form [9]. The edge-centered form is simple and intuitively based, and works particularly well when the fluid flow is close to grid-aligned; lower-dimensional symmetry properties are automatically captured. However, it contains no information about the zone topology. In contrast, the tensor form connects all points of a zone and gives better results when the fluid flow is far from being aligned with the grid; however, for highly elongated zones it can connect disparate zone length scales in an unphysical manner. The tensor form of the artificial viscosity is unchanged in its calculation in zones that contain nondynamical points. The edge-centered artificial viscosity is modified from the form given in [5] as follows: first, the density and sound speed used to compute this viscosity is taken to be the zone values, rather than from point-centered averages. This is done for all zones to obtain consistency across the mesh. Any change in the functional form of the artificial viscosity within the computational domain will itself result in errors for a steady-state shock even if there are no terminated lines. Second, the limiter function used with the viscosity calculated on the edge that connects the nondynamical point to that with a larger major radius, as shown in Fig. 1, is calculated as an average of that of the two limiters adjacent to it and oriented in the same direction. Thus for grid aligned flow in the radial direction in Fig. 1 these edges all have the same value for the limiter function. Other concerns about the artificial viscosity forces are discussed after presenting the numerical results that highlight difficulties that can occur with their use.

Finally, for completeness the trivial case of degenerate points is mentioned. Degenerate points occur at a center of convergence in 2D or 3D, or along the z-axis of a polar grid in 3D, where a set of points that are initially coincident are required to move together. In this case one simply adds the individually separate nodal masses and forces associated with these points for use in updating the common point velocity from the momentum equation. The change in specific internal energy of these zones need not be averaged as they are still separately Galilean invariant; however, this averaging can result in more robust results and is performed for the edge-centered artificial viscosity. An example of this is shown later with the Guderley test problem [11] utilizing a mesh with a center of convergence that is displaced along the z-axis, and moves when it encounters a converging shock wave.

4. Numerical results

The numerical results given next are of two types: sanity checks that gauge the effect of our donation procedure for two driven piston problems (a straight piston and the so-called Saltzman piston [12]), and more difficult tests utilizing the well-known Noh [13] and Guderley problems. The latter problems assess the size of errors in 1D symmetry, and the general robustness of the method in addition to its ability to keep the time-step from decreasing precipitiously. The results are computed with a 2D, unstructured grid code developed in the group T-7 at LANL [14,15]. A simple ideal gas law, $\gamma = 5/3$, equation of state is employed to compute pressures. An advection-type limiter is utilized to restrict the magnitude of both forms of artificial viscosity that are employed, edge-centered [5] and tensor [9], unless otherwise indicated.

We begin with a straight piston problem whose initial grid is shown in Fig. 5. The grid is on a domain of unit horizontal length and with a width of 0.1 in the ignorable, vertical direction with 101 equally spaced vertical lines and 21 equally spaced horizontal lines, one-half of which terminate at the middle of the domain. Thus the zones in the coarser region on the left half of the figure have one to one aspect ratio, and those in the finer region on the right half have 2:1 aspect ratio, elongated in the vertical direction. The initial density

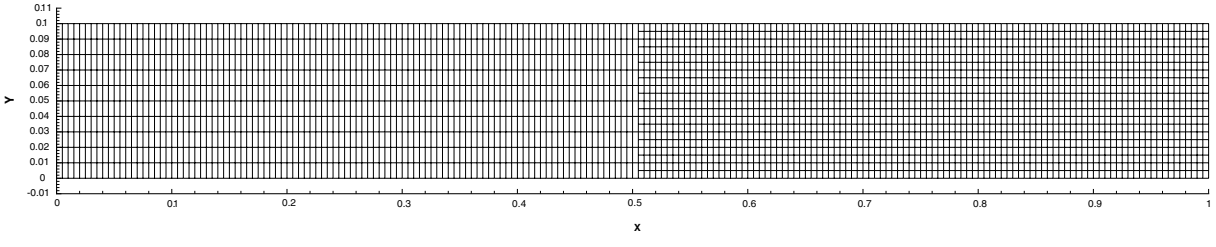

Fig. 5. Straight piston with termination lines – initial mesh.

is unity, with zero initial specific internal energy; the left piston boundary moves to the right with unit velocity driving a shock wave into cold media and across the terminated lines. Results showing the grid and density isolines at time $t = 0.6$ using the edge-centered viscosity are given in Fig. 6 parts (a) and (b): part (a) shows the result obtained with no modifications about the terminated lines, and part (b) presents results obtained if the mass and force donation procedure is performed. In the first instance the perturbations caused by the shock wave crossing the layer of terminated lines is clearly visible at the shock front that has moved far to the right of this layer. In part (b) these perturbations are totally absent; there are also no residual density changes at the termination layer. That is, the presence of terminated lines causes no perturbations to the solution, which is the same as though these lines were totally absent. With the use of the tensor artificial viscosity similar results are also seen; perturbations in the density are somewhat smaller than those in Fig. 6(a), but are still clearly visible; they are removed by the donation procedure. No subzone pressure forces are utilized, as these are unnecessary for this type of problem.

Next the initial grid shown in Fig. 5 is given the standard Saltzman perturbation to obtain the one displayed as Fig. 7. This problem is rerun with subzone pressure forces using a merit factor, $M_f = 1.0$. In Fig. 8 results are given at time $t = 0.6$ for four cases: parts (a) and (b) show the grid and density contours without, and with, modification for points at the termination layer, respectively, using the edge-centered artificial viscosity. These two figures are almost identical, and thus the donation procedure did not result in an improved solution but it also did not degrade it. In parts (c) and (d) are shown the results using the tensor artificial viscosity without, and with, modification for points at the termination layer. In this case the mass and force donations at the

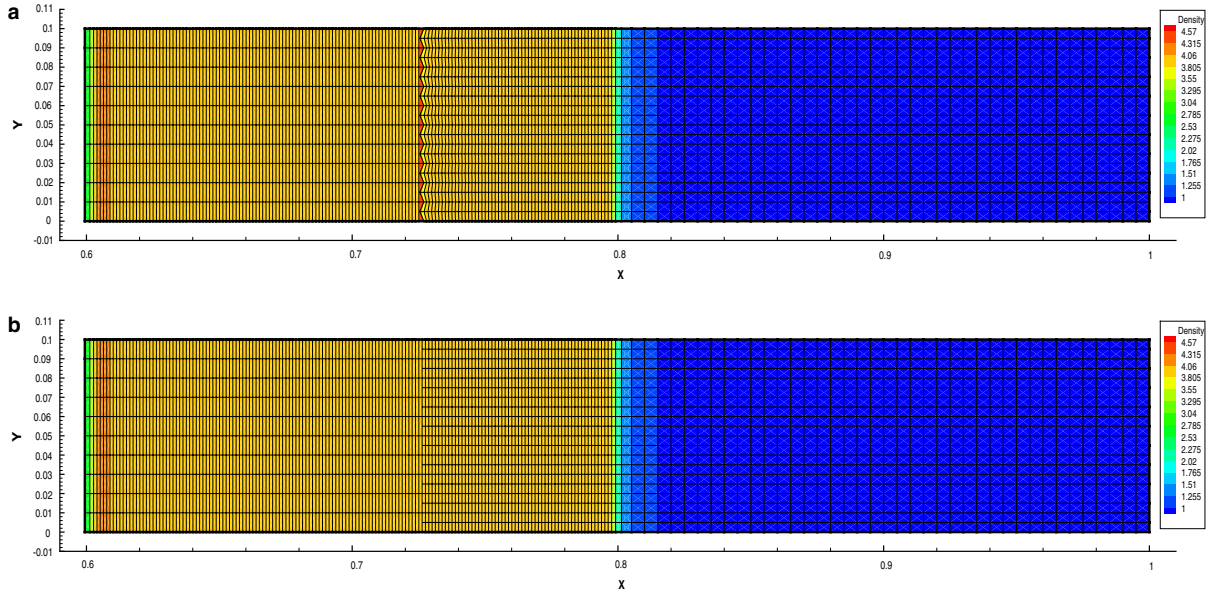

Fig. 6. Straight piston with termination lines for the edge viscosity – (a) mesh and density at $t = 0.6$ original code; (b) mesh and density at $t = 0.6$ with donation.

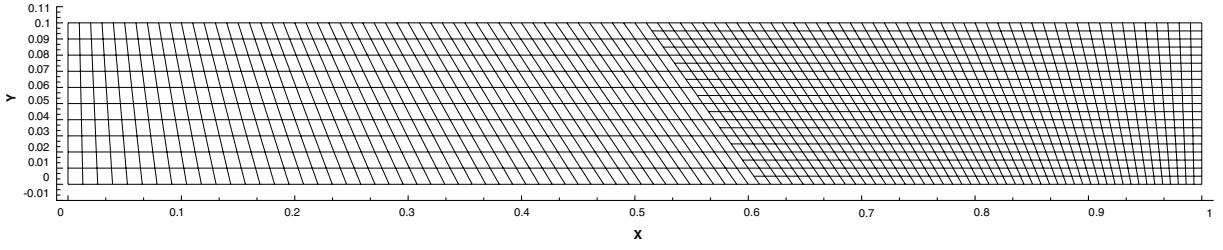

Fig. 7. Saltzman piston with termination lines – initial mesh.

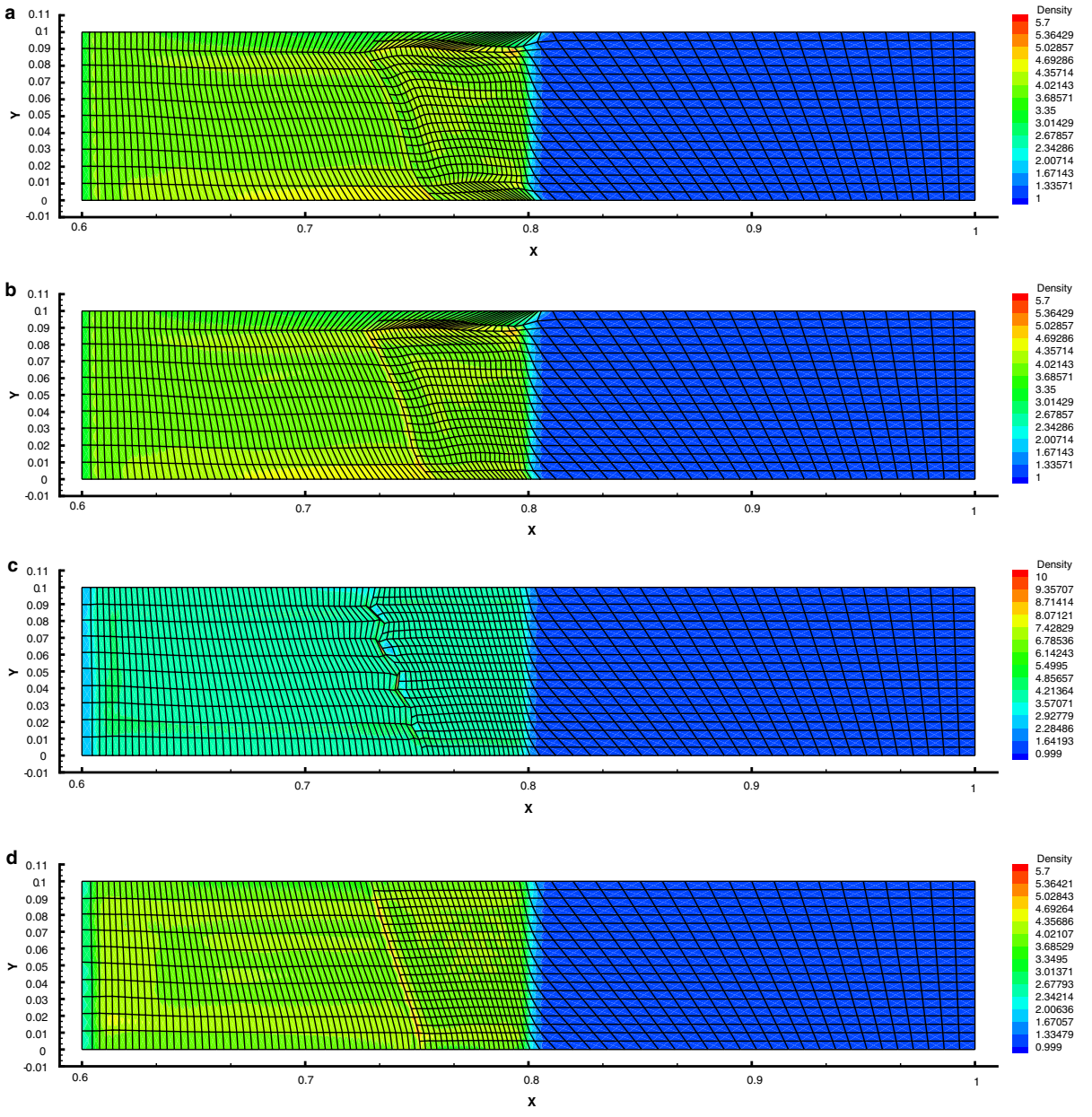

Fig. 8. Saltzman piston with terminated lines – mesh and density at $t = 0.6$: (a) edge viscosity original code, (b) edge viscosity with donation, (c) tensor viscosity original code, (d) tensor viscosity with donation – note different scales due to different behaviors.

termination layer result in a very substantial improvement. The shock front nearly breaks apart downstream of the termination layer and is close to failure without these modifications, but the results seen with them are better than those with the edge-centered viscosity. This problem also shows the necessity for averaging the work done on a timestep in the zones that share a common nondynamical point, which is a consequence of our third criterion that guarantees linear momentum conservation. If this averaging procedure is not carried out, negative specific internal energy is encountered in some of these zones and the calculation ends. It is only the sum of the work done into zones with a common nondynamical point that is positive.

The spherical Noh problem [13] is next considered in cylindrical geometry using area-weight differencing on an angular grid with one layer of terminated lines. The initial conditions are unit density, zero specific internal energy, and an inward radial velocity of magnitude 1.0. A spherical stagnation shock wave is generated and

travels outward from the center. Subzone pressure forces are turned off because they are not needed for this problem when run without terminated lines. The timestep is increased by a factor of two as expected with the single termination layer; for a high resolution simulation multiple termination layers are necessary. The simulation is performed to the point where the shock reaches the location of the first termination line at $t = 0.07866$. The grid at this time is shown in Fig. 9: parts (a) and (b) are without, and with, mass and force donation, respectively, using the edge-centered viscosity. A very large sawtooth-like oscillation occurs at the termination layer. This is largely, but not totally, removed by the enslavement procedure. Without subzone pressure forces the calculation in part (a) will not continue much longer; with them the grid distortion is somewhat reduced but not eliminated. In parts (c) and (d) are given the corresponding results for the tensor viscosity without, and with, the donation procedure, respectively. The grid without donation in part (c) is comparable in quality to that in part (b) for the edge-centered viscosity with donation. The symmetry errors in the density along the termination layer are detailed in Table 1. The donation procedure reduces these errors

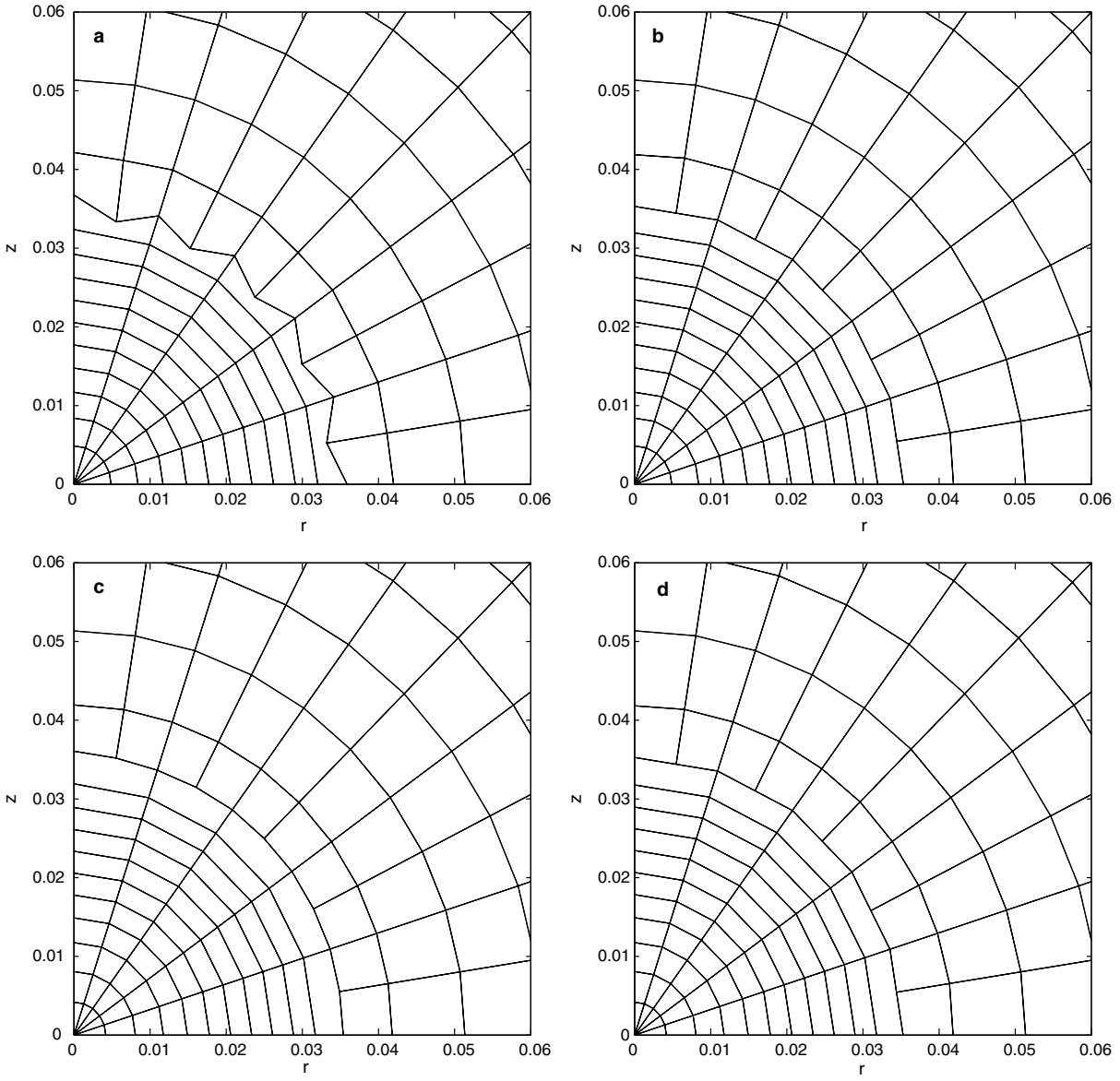

Fig. 9. Noh problem at $t = 0.07866$, the shock has just passed the termination line – final meshes (zoom): (a) edge viscosity, (b) edge viscosity with donation process, (c) tensor viscosity, (d) tensor viscosity with donation process.

Table 1
Noh problem: symmetry errors for edge and tensor viscosities along termination layer

$(\rho_{max} - \rho_{min})/\rho_{max}$	Original code	With donation
Edge viscosity	3.1×10^{-2}	4.0×10^{-4}
Tensor viscosity	4.5×10^{-2}	1.2×10^{-4}

to truncation levels, but recall that for no termination layer and area-weight differencing they are always at roundoff error level.

The last test problem considered is the driven spherical impulsion problem of Guderley [11]. This has an initial density of unity, zero specific internal energy, and a velocity boundary condition given in [6] using area-weight differencing in cylindrical geometry. Results are shown with two layers of terminated points, and for comparison without terminated lines, for two types of grid setups: first, with 51 equally-spaced radial and 51 equally-spaced angular divisions on a one-half circular domain of unit initial radius, with a center of convergence at ($r = 0$, $z = 0$); and second, the same total domain but with circular lines that have their centers moved along the z-axis such that the center of convergence is displaced to the point ($r = 0$, $z = 0.5$). In both cases the velocity boundary condition is the same, and the outer boundary remains a circle with center at ($r = 0$, $z = 0$). Subzone pressure forces with merit factor unity are utilized for both the centered and off-axis center of convergence cases. This problem is run to a time $t = 0.8$ at which point the shock wave has reached the true center of convergence, is propagating outward, and has recrossed the inner layer of terminated points. The results are seen in Fig. 10 where the top two parts show the grid and density isolines for no radially terminated layers. The bottom two parts give these same results with two terminated layers; the edge-centered artificial viscosity and the donation procedure at the termination layers are utilized. The results are very comparable in quality. The number of timesteps needed to run without and with terminations is about 3000 and 1000, respectively. It is this decrease in spatial grid stiffness without degradation in solution quality that the donation procedure is intended to produce. The tensor form of the artificial viscosity produces results of similar quality.

Finally, Fig. 11 shows the initial grid for the Guderley problem with the displaced center of convergence described previously, both with two layers of termination lines and without such points. Results are given in Fig. 12 utilizing the edge-centered viscosity for the case without, and with, termination layers; both the grid and the density isolines are shown at the final time of $t = 0.8$. Likewise, similar results are given for the tensor viscosity at the same final time in Fig. 13. The density bulge that results from the shock wave that is reflected from the true center of convergence of this problem at ($r = 0$, $z = 0$) is quite visible in both figures. With the edge-centered viscosity and no terminated lines it took about 9000 timesteps to run to completion, whereas with the two termination layers this was reduced to roughly 2000; for the tensor viscosity these values are approximately 6300 and 1700, respectively. Thus our donation procedure is effective in this regard. However, in order to make these displaced center of convergence cases run to completion the limiters were turned off on both forms of the artificial viscosity. Additionally, the velocity of points on the z-axis were enslaved to those points on the next radial line angularly outward (for area-weight differencing this causes no energy errors since these points carry zero mass [3].), rather than being moved dynamically as they are for the nondisplaced center of convergence case shown in Fig. 9. Usually simulations terminate due to very small timesteps just after the shock wave intersects the false center of convergence without this set of alterations. This can be changed somewhat depending on the value of the merit factor that multiplies the subzone pressure forces. Generally the tensor form of the artificial viscosity shows more robustness and better quality of results for the case of very nongrid-aligned flow than the edge-centered form, which agrees with the results presented in [9]. This rather unsatisfactory state of affairs is due to the lack of a consistent form of the artificial viscosity that is optimal for all simulations. This topic is addressed next.

4.1. Artificial viscosity forces

The artificial viscosity forces that are necessary to resolve shocks in the otherwise dissipationless Euler equations that are solved herein have been the subject of much discussion and controversy since they were introduced many years ago [16]. While there is still no universal agreement on the precise functional form for these forces, they can usually be viewed as variations on the basic form expressed in [17] as

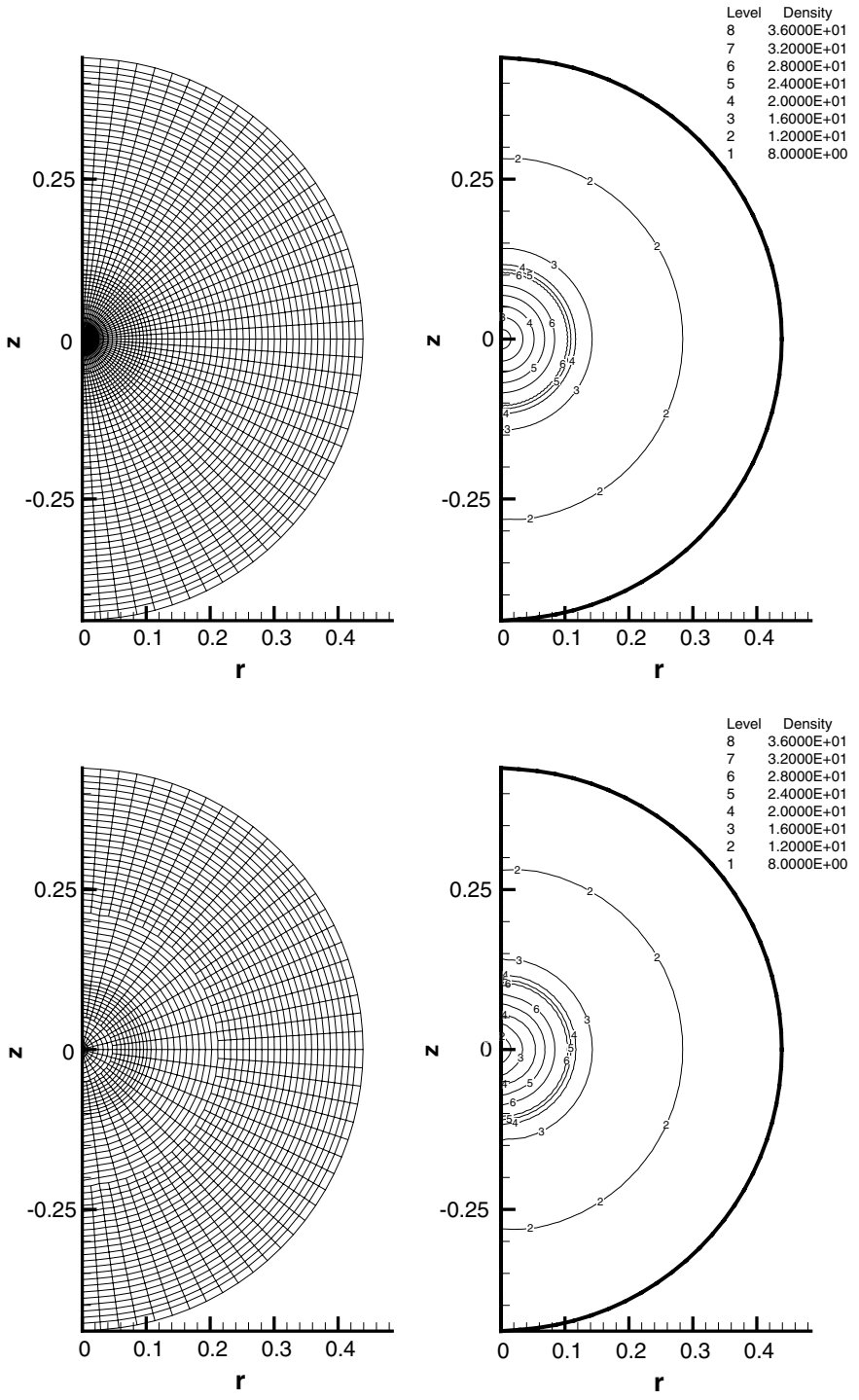

Fig. 10. Guderley problem at $t = 0.8$ with edge viscosity. Top: final mesh and density isolines with no termination layers; Bottom: two termination layer final mesh and density isolines.

$$q_z = \rho[c_s \Delta v + (\Delta v)^2], \tag{4.1}$$

where "q_z" acts as an addition to the scalar pressure of zone "z", with the additional requirement that the zone be under compression for the forces to be dissipative. The factor "ρ" is a measure of density, "c_s" is a sound

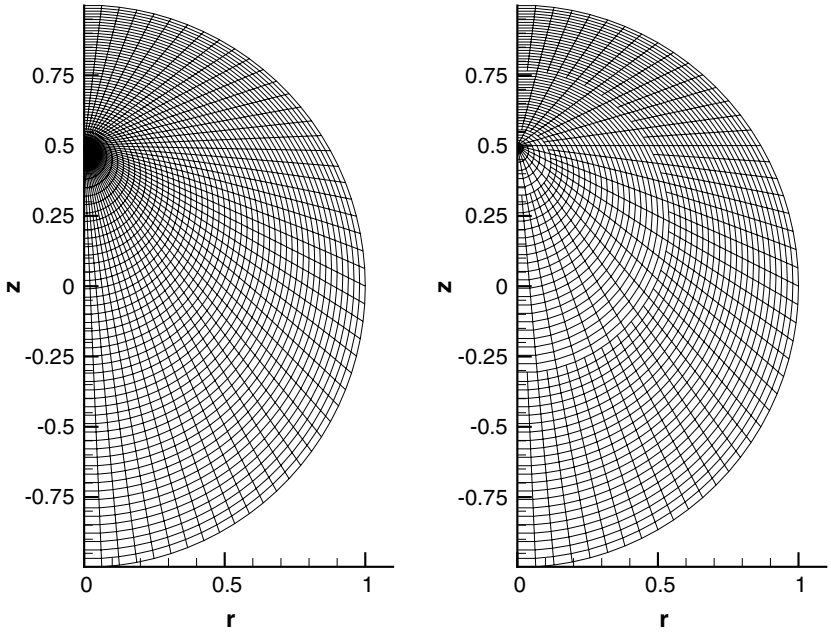

Fig. 11. Initial meshes for Guderley problem with displaced grid center of convergence. Left: without terminations (51×51) circular and radial lines; Right: two termination layers.

speed, and "Δv" is a jump in the magnitude of the velocity about a zone; all of these can be calculated in more than one manner. The two terms on the RHS of Eq. (4.1) are referred to as the linear and nonlinear artificial viscosity, respectively.

Ideally one wishes to solve the Euler equations by integrating along the characteristics of this hyperbolic system. However, because this is both too difficult, and too expensive to compute, one resorts to shock capturing methods by inserting an artificial viscosity term that regularizes the discontinuities that otherwise occur. This term may be inserted directly as done herein, or as the consequence of solving a local Riemann problem, with much the same effect. With the former approach, more recent forms of the artificial viscosity term that give much improved results over older versions, are developed by specifying conditions under which the characteristics of the Euler equations do not cross, and thus where dissipation is not needed. This results in the inclusion of a limiter function that augments the compression switch in the basic artificial viscosity, Eq. (4.1). The limiter has the form of that used for advection except that the "upwind" direction of material advection is unimportant, and also, it should not limit the magnitude of these forces so much that oscillations occur behind a strong shock. The purpose of the limiter in this context is to turn off the artificial viscosity for adiabatic compression, or along a front of constant phase where the edge-projected velocity field is a linear function of the coordinates, and thus where the characteristics of the hyperbolic system do not cross. However, for general flow that is nongrid-aligned there is no theory that indicates how this limiter should be constructed. It can simply result in a decreased value of these forces that degrades overall robustness of the calculations, as occurs with the above simulations.

For the terminated line situation considered in this paper, there is a more fundamental difficulty when the artificial viscosity is computed using the velocity of a nondynamical point that has been set by linear interpolation. As is seen from Eq. (4.1), a linear interpolation of the velocity from two dynamical points to one nondynamical point results in a decrease in the strength of the linear viscosity term by one-half, and the nonlinear term by one-quarter. This situation gets geometrically worse for the case of multiple terminations. Furthermore, the limiter function defined along these edges is invalid since a limiter calculated from a linearly interpolated velocity will always turn completely off. The zone-centered tensor artificial viscosity also exhibits this problem, although in some averaged sense that is more difficult to quantify. One can separately reconstruct the edge-centered viscosity without using the points that have interpolated velocities. This is the

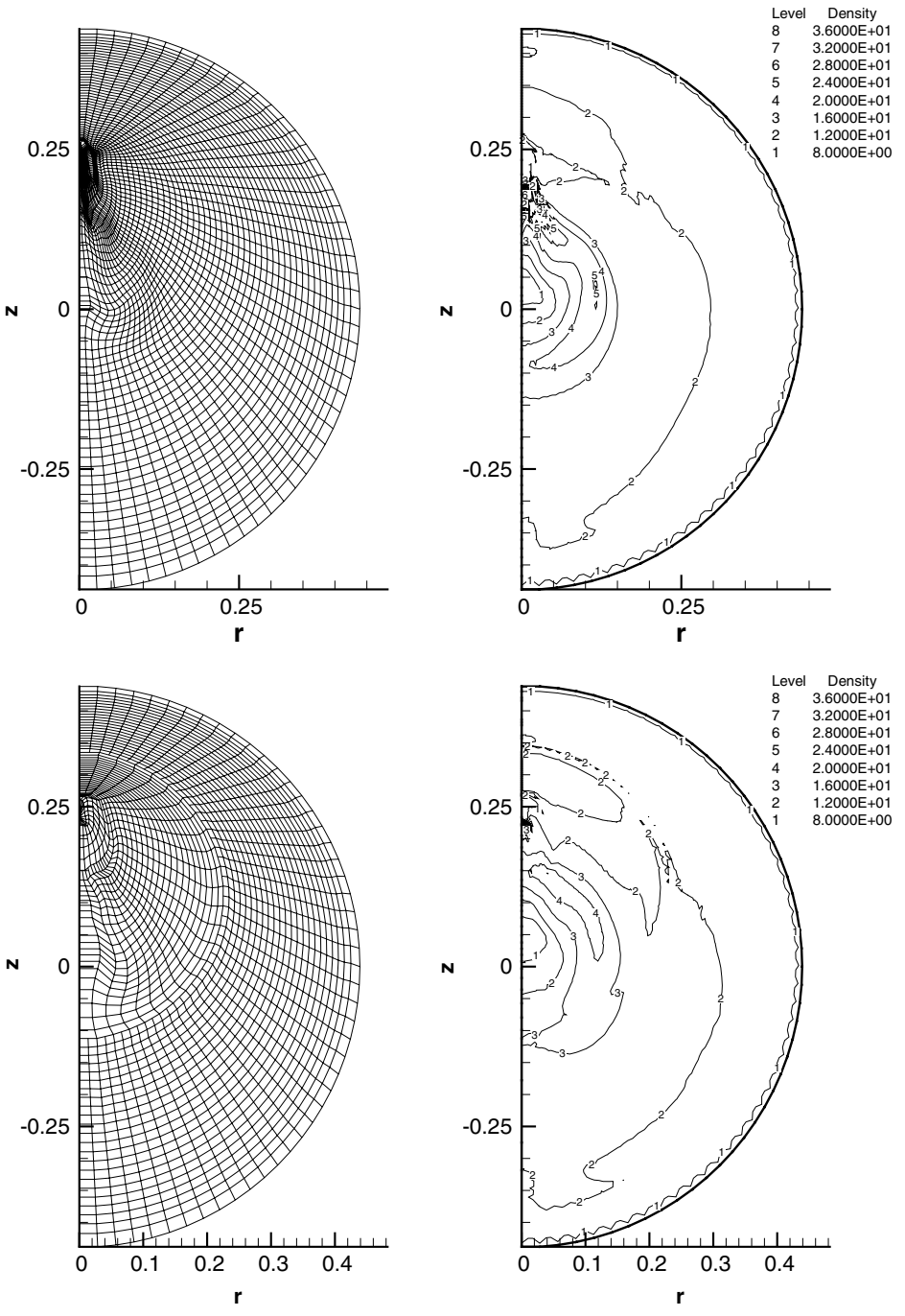

Fig. 12. Guderley displaced center problem at $t = 0.8$ with the edge viscosity. Top: final mesh and density isolines; Bottom: two termination layers, final mesh and density isolines – with donation.

ideal solution, but one that is expensive computationally. The treatment of the artificial viscosity is found to be problematical in that changes in zones that contain nondynamical points may be mirrored as errors (severe zone volume collapse) in regular neighboring zones that do not contain these modifications. There is no known ''optimal'' form of the artificial viscosity, and the inclusion of this term into the Euler equations is always fraught with difficulties.

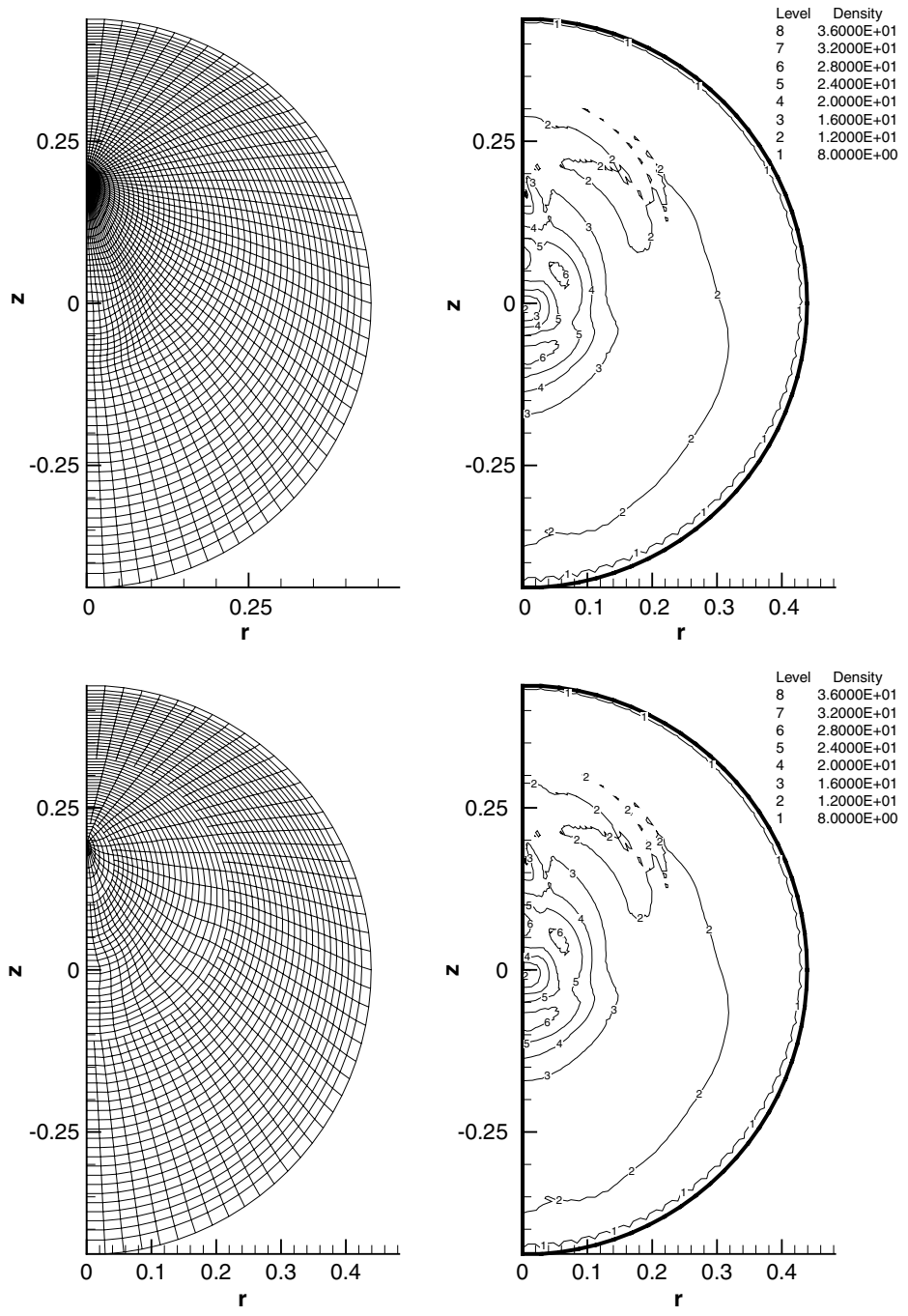

Fig. 13. Guderley displaced center problem at $t = 0.8$ with the tensor viscosity. Top: final mesh and density isolines; Bottom: two termination layers, final mesh and density isolines – with donation.

5. Discussion and conclusions

The purpose of this work is twofold: first, to complete the compatible formulation of Lagrangian hydrodynamics by addressing the remaining finite-volume discretization questions that arise when treating grid points that must be internally enslaved within the grid to prevent timestep collapse; and second, to address

certain more general questions concerning the basic structure and implementation of this numerical algorithm. That these issues are related is seen in Section 3. There it is shown that the types of grids that must be used to reduce numerical perturbations about exceptional points involve a restriction of the type of zone to be uniform across the grid. This is seen in going from Fig. 4(a) to (b) where a pentagon becomes a quadrilateral. A compelling reason for using a restricted set of zone types is that the central quantity that must be computed to implement this algorithm is the corner force. If one knows that the number of corners of all the zones is the same, then sweeps over all zones, combined with sweeps over the known number of internal zone edges and corners, allows the corner force to be assembled with computer code that is simple to construct, and which executes in an efficient manner.

It was shown that the basic discretization about exceptional, or nondynamical, points could be largely handled by three basic rules that involve already computed corner masses and forces so that the number of additional operations is small. These involved impedance matching of corner volumes and masses by donation to nearby dynamical points to which the velocity of the nondynamical points is enslaved. An appropriate addition of the remaining corner forces, after median mesh grid adjustment, and their subsequent division and donation to neighboring dynamical points is performed such that force equilibrium is achieved for uniform stress (a necessary sanity check). It was shown that for the internal energy equation to obey momentum conservation about nondynamical points, it is required that the definition of what region in space constitutes a "zone" be generalized. A zone becomes the smallest region in space for which its associated corner forces sum to zero. Thus, primitive zones that contain common nondynamical points must be lumped together in calculating the work term in the internal energy equation. Numerical results were shown to validate the procedures given, and to quantify the magnitude of the errors that necessarily occur with the introduction of terminated lines and their associated nondynamical points. Artificial viscosity forces are always the most crucial component of any shock-wave hydro algorithm. There is still no universally satisfactory form of the artificial viscosity suitable for all problems. The fact that different forms for this force are often utilized depending on the type of problem being studied is the major remaining deficiency of this class of hydrodynamics methods.

Finally, the discrete, compatible formulation of Lagrangian hydrodynamics was developed in a manner that explicitly displays the nature of this algorithm to be that of an algebraic identity. This identity consists of two arbitrary scalars, the zone and point masses, and one arbitrary vector, the corner force, such that the usual definition of total energy conservation is always exact. This algorithm thus reveals itself to be a true tautology in the sense described in [18]. As such, it describes a priori truth that cannot be confuted, since in primitive form it makes no assertion about any physical system. As remarked in [18], tautologies are neither trivial nor useless, but embody the kernel from which physical systems of truth may be constructed. Thus the quality with which the discrete, compatible formulation of Lagrangian hydrodynamics may describe certain physical situations is mostly, if not entirely, dependent on the quality of the specification of the three abstract quantities that compose it.

Acknowledgements

All numerical simulations were performed using ALE INC [standing for ALE INC(ubator)], a 2D Arbitrary-Lagrangian–Eulerian code that utilizes general polygonal grids, and which was developed in the Mathematical Modelling and Analysis Group (T-7) at LANL [14,15]. The authors wish to thank M. Shashkov for fruitful discussions, and the referees for their helpful comments. This work was supported by the Advanced Strategic Computing program of the US Department of Energy.

References

[1] E.J. Caramana, Timestep relaxation with symmetry preservation on high aspect-ratio angular or tapered grids, J. Comput. Phys. 166 (2001) 173–185.

[2] D.E. Burton, Exact conservation of energy and momentum in staggered-grid hydrodynamics with arbitrary connectivity, in: Advances in the Free Lagrange Method, Springer Verlag, New York, 1990.

[3] E.J. Caramana, D.E. Burton, M.J. Shashkov, P.P. Whalen, The construction of compatible hydrodynamics algorithms utilizing conservation of total energy, J. Comput. Phys. 146 (1998) 227–262.

[4] B. Alder, S. Fernbach, M. Rotenberg (Eds.), Methods in Computational Physics, vol. 3, 1964.

[5] E.J. Caramana, M.J. Shashkov, P.P. Whalen, Formulations of artificial viscosity for multi-dimensional shock wave computations, J. Comput. Phys. 144 (1998) 70–97.
[6] E.J. Caramana, M.J. Shashkov, Elimination of artificial grid distortion and hourglass-type motions by means of lagrangian subzonal masses and pressures, J. Comput. Phys. 142 (1998) 521–561.
[7] E.J. Caramana, P.P. Whalen, Numerical preservation of symmetry properties of continuum problems, J. Comput. Phys. 141 (1998) 174–198.
[8] E.J. Caramana, C.L. Rousculp, D.E. Burton, A compatible, energy and symmetry preserving lagrangian hydrodynamics algorithm in three-dimensional cartesian geometry, J. Comput. Phys. 157 (2000) 89–119.
[9] J.C. Campbell, M.J. Shashkov, A tensor artificial viscosity using a mimetic finite difference algorithm, J. Comput. Phys. 172 (2001) 739–765.
[10] C. Lanczos, The Variational Principles of Mechanics, fourth ed., Dover Publications, 1986, p. 384.
[11] R. Lazarus, Self-similar solutions for converging shocks and collapsing cavities, SIAM J. Numer. Anal. 18 (1981) 316.
[12] J.K. Dukowicz, B. Meltz, Vorticity errors in multidimensional Lagrangian codes, J. Comput. Phys. 99 (1992) 115.
[13] W.F. Noh, Errors for calculations of strong shocks using an artificial viscosity and an artificial heat flux, J. Comput. Phys. 72 (1987) 78.
[14] J. Campbell, M. Shashkov, A compatible lagrangian hydrodynamics algorithm for unstructured grids, Selcuk J. Appl. Math. 4 (2003) 53–70, Report version can be found at <http://cnls.lanl.gov/~shashkov>.
[15] R. Loubere, First steps into ALE INC(ubator). A 2D ARBITRARY-LAGRANGIAN-EULERIAN CODE ON GENERAL POLYGONAL MESH FOR COMPRESSIBLE FLOWS Version 1.0.0, Los Alamos National Laboratory Report, LA-UR-04-8840.
[16] J. VonNeumann, R.D. Richtmyer, A method for the calculation of hydrodynamic shocks, J. Appl. Phys. 21 (1950) 232–237.
[17] M.L. Wilkins, Use of artificial viscosity in multidimensional shock wave problems, J. Comput. Phys. 36 (1980) 281–303.
[18] A.J. Ayers, Language, Truth, and Logic, Dover Publications, 1952, pp. 84–87.